JPEDAV (2010) 31:223–232
DOI: 10.1007/s11669-010-9693-9
1547-7037 ©ASM International

Determination of the Diffusivity of Point Defects in Passive Films on NiTi and NiTiAl Alloys

Kuan-Ting Liu and Jenq-Gong Duh

(Submitted April 6, 2009; in revised form January 7, 2010)

A point defect model based on the movement of cation and anion defects in an electrostatic field was carried out to explain the growth and dissolution behavior of a passivation layer on NiTi and NiTiAl thin films. The calculated value of diffusivity was in range of 10^{-16} to 10^{-17} cm^2/s. The defect of oxygen vacancy revealed that the passive film was an n-type semiconductor. Mott-Schottky analysis showed that the doping level within a passive film was rather large and in the order of 10^{20} to 10^{21} cm^{-3} film, which was considered to be a highly doped structure. The high-resolution transmission electron microscopy (HRTEM) images showed that the highly doped structure consisted of amorphous and crystalline structures of TiO_2 and Al_2O_3, respectively. A thermodynamic evaluation for the difference between crystalline and the fully amorphous oxides was calculated to be 57.57 and 96.87 kJ/mol, respectively. In the amorphous region, the electronic level arises from the presence of an energy band gap in the ideal crystalline structure. Therefore, the smaller donor density and the lower diffusion coefficient retarded the defect movement in the passivation layer, and improved the stability of the passive film during corrosion.

Keywords diffusivity, Mott-Schottky, NiTi, NiTiAl, passivation film, point defect model

1. Introduction

Passivity is the spontaneous formation of a thin oxide film (the passive layer) in a particular environment. The oxide film can decrease the corrosion rate by many orders of magnitude.[1,2] The oxide films are formed on nearly all metal surfaces subjected to oxidative environments. In the literature,[3,4] the growth of oxide films is controlled by the rate of transport of cationic species through the film. The driving force of migration is described by a high-field mechanism, which is exponentially related to the local electric field. Transport in an oxide film can be explained in terms of mobile vacancies and defects, resulting in the penetration of the oxide film into the metal surface. On the other hand, metal ions are transported in the reverse direction with the relative fluxes of these species with respect to the energetics of formation for specific vacancies.[5] Recently, studies with the use of a defect model emphasized that current is conducted by mobile charged defects.[6–10] Macdonald's point defect models (PDMs)[7–10] use the elementary vacancy generation and annihilation reactions at the interface as a basis. It provides an atomic scale of growth and breakdown for passivation films under steady state and transient conditions. The effect of the electrostatic field drives the migration of point defects (oxygen and metal vacancies). The main factor for involving the transport properties of oxygen vacancies and hence the kinetics of film growth is dominated by the vacancy diffusivity.

The semiconductor properties and electronic structure of a passive film can vary over a wide range with respect to the alloy composition, microstructure, film thickness, defect, and ionic conductivity.[11] The band structure model can be employed to explain the oxidation processes in terms of lattice ionic defects and the oxide film growth mechanism. For the general case of a defect oxide grown on a metal, the space charge region can accompany in the oxide. Especially, many oxide passive films are characterized by a high doping level with a large concentration of localized states within the band gap. The vacancy concentrations may be as larger as 10^{20} cm^{-3}, if it is assumed that the defects act as the dopants (oxygen vacancies $V_{\ddot{O}}$ and cation vacancies V_M, indicating n-type and p-type character, respectively).[12,13] Since film formation and dissolution involve the movement of ions and electrons, electronic properties reveal one of the most significant characterizations of a passivation film to its corrosion resistance, which may be an important factor in the film breakdown mechanism. The transport properties of defect can be expressed quantitatively by their vacancy

This paper was presented at the Diffusion in Materials for Energy Technologies Symposium held in San Francisco, CA, USA, February 15-19, 2009. This symposium was co-sponsored by the Alloy Phase Committee of the joint EMPMD/SMD of TMS, the TMS High Temperature Alloys Committee, the TMS/ASM Nuclear Materials Committee, the TMS Solidification Committee, and the ASM-MSCTS Atomic Transport Committee. The symposium was organized by J.C. Lacombe of the University of Nevada, Reno; Y.H. Sohn of the University of Central Florida; C. Campbell of the National Institute of Standards and Technology; A. Lupulescu of the General Electric Company; and J.-C. Zhao of the Ohio State University.

Kuan-Ting Liu and **Jenq-Gong Duh**, Department of Materials Science and Engineering, National Tsing-Hua University, Hsinchu, Taiwan. Contact e-mail: jgd@mx.nthu.edu.tw.

diffusivity (D_v). Therefore, quantitative analysis of the PDM on the concentration and transport properties of vacancies can be employed to evaluate the diffusivity of a point defect (D_v) in the passive film, assuming the Nerst-Planck formulation.[5] Bojinov[14] used a surface charge approach to calculate the diffusivity of oxygen vacancies in a passive film on tungsten. Luo and coworkers[15] and Ahn and Kwon[16] also determined D_v on the Fe-based substrate on the basis of the idea of the PDM.

Ti-Ni alloys have been extensively studied and are the most important commercial shape-memory alloys because of their exclusive shape-memory performance and excellent mechanical properties. Besides, the alloys exhibit good corrosion resistance and biocompatibility, and this leads to their wide use in the biomedical applications.

The corrosion resistance of NiTi and NiTiAl film was stressed with respect to the grain size effect.[17] The nano-size effect in corrosion resistance can be attributed to the fast diffusion of metal in the grain boundary, which forms a protective passive layer, leading to enhancement in both the kinetics of passive layer and the stability of the passive film formed. However, there is still lack of diffusivity data for point defects in the passive films formed on NiTi and NiTiAl.

In this work, the Mott-Schottky (M-S) analysis of NiTi and NiTiAl in chloride solution was performed and the dopant (defects) concentration was measured as a function of the film formation potential. The relationship between the donor density and the film formation potential was discussed in order to understand the passivation behavior of NiTi and NiTiAl. In addition, the microstructure of the passive films was investigated by HRTEM to correlate the electronic structure of the passive films with the characterization of defects.

2. PDM Theory

Mass transfer to an electrode is governed by the Nernst-Planck equation.[18] For the one-dimensional mass transfer along the x-axis

$$J_i(x) = -D_i \frac{\partial C_i(x)}{\partial x} - \frac{z_i F}{RT} D_i C_i \frac{\partial \Phi(x)}{\partial x}, \qquad \text{(Eq 1)}$$

where J_i is the flux of species i (mol s^{-1} cm^{-2}) at distance from the surface; D_i is the diffusion coefficient (cm^2/s); $\frac{\partial C_i(x)}{\partial x}$ is the concentration gradient; z_i and C_i are the charge and concentration (mol cm^{-3}) of species i, respectively; and $\frac{\partial \Phi(x)}{\partial x}$ is the external electrical field.

To consider a compound MX with an external electrical field as $\varepsilon = -\frac{\partial \Phi(x)}{\partial x}$, Eq 1 is rewritten as (2) and (3) for cations and vacancies, respectively.

$$J_M(x) = -D_M \left(\frac{\partial C_M}{\partial x} - \frac{z_M F \varepsilon}{RT} C_M \right) \qquad \text{(Eq 2)}$$

$$J_v(x) = -D_v \left(\frac{\partial C_v}{\partial x} - \frac{z_v F \varepsilon}{RT} C_v \right) \qquad \text{(Eq 3)}$$

The detailed explanation of PDM has been discussed in literature.[7-10,19] Macdonald and coworkers[5] concluded that the density of donors (N_d) is given as

$$C_v(L_{ss}) = N_d = \omega_1 \exp[-bU_{ff}] + \omega_2, \qquad \text{(Eq 4)}$$

where $C_v(L_{ss})$ is the concentration of vacancies at the metal/film interface, wherein they are created; N_d, the density of donors in the passive film; ω_i and b, the unknown constants to be fitted in experiment; and U_{ff}, the film formation potential.

ω_2 is given by

$$\omega_2 = \frac{J_v RT}{zFV_0 D_v}, \qquad \text{(Eq 5)}$$

where J_v is the steady-state flux of donors; V_0, the mean electric field strength; R, the gas constant; T, the temperature; and F, the Faraday constant.

3. Experimental Procedure

NiTi and NiTiAl thin films were prepared with a mixed NiTi and a single aluminum target by using DC magnetron sputtering. The purity of NiTi alloy (50.6at.%Ti-49.4at.%Ni) target and aluminum target with 2 in. diameter were 99.95% and 99.99% pure, respectively. The Si substrate was not heated so that the amorphous structure of the as-deposited thin films could be achieved. The amorphous thin films were subjected to annealing process and then transformed into crystallization. In the previous study,[19] the annealing temperatures were selected as 798 K for 1 h under a vacuum of nearly 5×10^{-5} torr (6.7×10^{-3} Pa). The compositions of thin films were quantitatively measured with an electron probe microanalyzer (EPMA JXA-8800M, JEOL) with the aid of a ZAF (Z = atomic number factor, A = absorption factor, F = characteristic fluorescence correction) program. The counting of the activated intensity in the tested specimen was compared to the pure Ni, Ti, and Al standards. For quantitative analysis, the accelerating voltages of EPMA were controlled at 15 kV. In addition, the microstructure of passive films was also investigated by high-resolution transmission electron microscopy (HRTEM-3000F, JEOL, Tokyo, Japan).

The corrosion experiments were performed in a conventional three-electrode electrochemical cell. A saturated calomel electrode (SCE) was used as the reference electrode and all potentials listed were referred to SCE. A carbon rod was used as the counter electrode. The specimens were pre-passivated at various potentials (film formation potential), and then the capacitance was determined by performing a potential scan in the anodic direction with a model 273A potentiostat/galvanostat (EG&G) corrosion measurement system. The film formation time for all specimens was 30 min. The measurement frequency was 1000 Hz. Prior to all experiments, the working electrode was cathodically prepolarized at −1 V for 300 s to remove oxide film formed in air. The test area was fixed at 0.5 cm^2 and the electrolyte was the chloride-containing pH 7 solution with 0.9% NaCl.

The in-depth distributions of passive films were characterized by a ESCA PHI 700 spectrometer with Al K_α x-ray source. The normalized binding energies with respect to that of C 1s peak at 285.0 eV were used to calibrate the XPS spectra for charge shifts. XPS depth profiles were determined using Ar^+ ion sputtering gun at 3 keV.

4. Results and Discussion

4.1 X-Ray Photoelectron Spectroscopy and HRTEM Analysis

Passive films are formed on many alloys which exhibit semiconductor properties due to effect of defects. The electrochemical studies can provide some interesting insights into the electronic structure between the passive film and electrolyte, and this can be related to the mechanism of formation and the breakdown of the passive films. XPS analysis was conducted on the $Ni_{50.5}Ti_{49.5}$ and $Ni_{45.6}Ti_{49.3}Al_{5.1}$ films, as shown in Fig. 1 and 2, respectively. Figure 1 presents the XPS spectra of O 1s, Ti 2p, and Ni 2p obtained from the corrosion surface of $Ni_{50.5}Ti_{49.5}$ under potentiostatic treatment at 500 mV_{sce} for 30 min. For the as-received state, the most outer layer was identified as Ti^{4+} state corresponding to Ti $2p_{3/2}$ peak at 459.1 eV. During depth profiling, the XPS spectra of Ti were broadened because TiO_2 was partly reduced to suboxide states. The presence of suboxides beneath the outer layer TiO_2 was Ti_2O_3 and TiO. In Fig. 2, the XPS spectra showed O 1s, Ti 2p, Ni 2p, and Al 2p scans on the surface of $Ni_{45.6}Ti_{49.3}Al_{5.1}$. The XPS spectra of Ti revealed the same behavior as Fig. 1(b), in which the Ti oxide layer contained Ti suboxides below TiO_2. The XPS spectra of Al $2p_{3/2}$ were located at 74.6 eV, denoting the formation of Al_2O_3 under 30s and 90s depth profiling. However, for the as-received state, the Al^{3+} peak was not evident, as shown in Fig. 2(d). For binary $Ni_{50.5}Ti_{49.5}$ alloy system, the outer passive layer is mainly composed of TiO_2 and then Ti_xO_y formed within the oxide layer. The XPS analysis revealed the passive film consisting of inner layer with TiO, Ti_2O_3 and outer layer with TiO_2 and Al_2O_3 on the surface of $Ni_{45.6}Ti_{49.3}Al_{5.1}$. Nevertheless, the nickel oxide, including NiO and Ni_2O_3, were not observed. Titanium exhibits preferential oxidation due to thermodynamic reasons: the free energy of formation ΔG (298 K) for NiO, TiO, TiO_2, and Al_2O_3 is -211.7, -495, -889.5, and -1581.7 kJ mol^{-1}.[20] The schematic plots of the passive layer on the surface of $Ni_{50.5}Ti_{49.5}$ and $Ni_{45.6}Ti_{49.3}Al_{5.1}$ were given in literature.[17] It was suggested that Al^{3+} ions entered Ti lattice as interstitial substituents.[21] Al^{3+} can be incorporated within or on top of the TiO_2 layer due to the potential-dependent effect.

Figure 3(a) shows the HRTEM bright field image of an analyzed passive film on the $Ni_{45.6}Ti_{49.3}Al_{5.1}$ under potentiostatic treatment at 500 mV_{sce} for 30 min. It appeared that

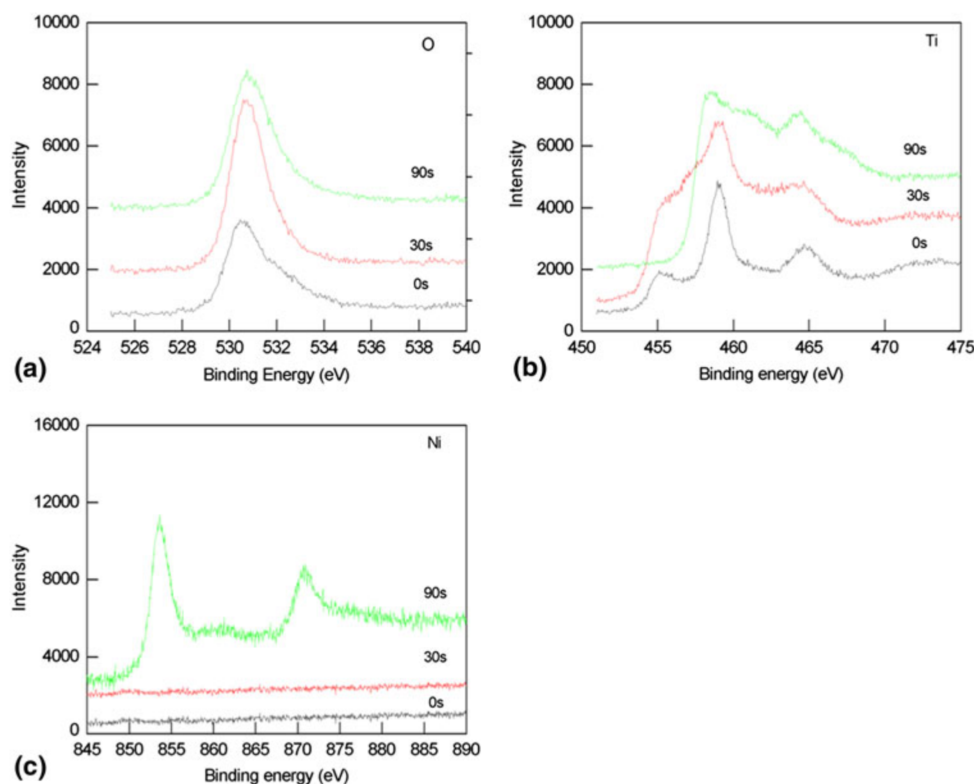

Fig. 1 XPS depth profile of $Ni_{50.5}Ti_{49.5}$ photo-peaks after 1800 s of growth at 500 mV (vs. SCE) in chloride-containing solution. (a) O 1s; (b) Ti 2p; (c) Ni 2p

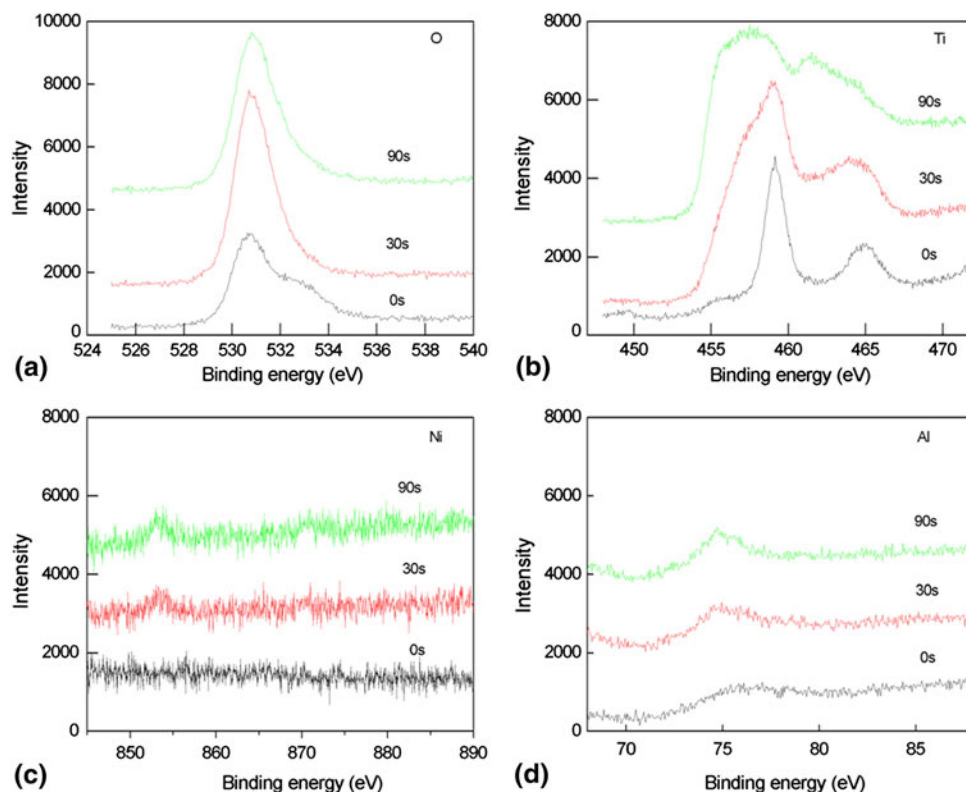

Fig. 2 XPS depth profile of $Ni_{45.6}Ti_{49.3}Al_{5.1}$ photo-peaks after 1800 s of growth at 500 mV (vs. SCE) in chloride-containing solution. (a) O 1s; (b) Ti 2p; (c) Ni 2p; (d) Al 2p

two passive films formed on the surface of $Ni_{45.6}Ti_{49.3}Al_{5.1}$. The passive A and passive B were denoted as two distinct layers. The total thickness of two passive films was determined by HRTEM to be 26 nm. The highly magnified image of HRTEM in passive A region is shown in Fig. 3(b). The amorphous structure prevailed in the passive A layer. In addition, regions 1, 2, and 3 were also analyzed by EDS, as listed in Table 1. In these three regions, the Ti-rich stoichiometry was measured with as average of 40.1 at.% within the amorphous oxide. The higher magnification of HRTEM image in passive B is represented in Fig. 3(c). In this layer, some lattice images can be observed, as indicated in regions 1 and 2. The amorphous and crystalline structures coexisted in the passive B layer. Regions 1, 2, and 3 were also selected to measure the composition by TEM-EDX, as indicated in Table 2. For regions 1 and 2, the Al-rich oxide existed in the crystalline structure. In region 3, the composition of 37.3 at.% Ti, 6.3 at.% Al, and 56.5 at.% O was detected in the amorphous phase. In general, passive films exhibited the mixed features of amorphous and crystalline structure. The structure of the passive layer is not only critical to determine the diffusivity of point defect, but also influences the electronic structure. In this study, the passive structure of $Ni_{45.6}Ti_{49.3}Al_{5.1}$ was investigated by HRTEM. The images showed that the amorphous and crystalline structures coexisted. Especially, the Al-rich and Ti-rich stoichiometry can result in the crystalline and amorphous region, respectively.

The electronic states in the semiconductor can be described by the band model. According to Peterson and Parkinson,[22] amorphous semiconductors are characterized by a high density of states localized between the valence and the conduction bands. Thus, amorphous semiconductor are expected to have a more continuous distribution of surface states between valence and conduction bands than a crystalline material due to the variation in bond lengths in the lattice. For the real passive film with amorphous or highly defective state, the model of an intrinsic semiconductor should be modified, as shown in Fig. 10. The electronic level is characterized by the presence of an energy band gap for ideal crystalline structure, as indicated in Fig. 4. If the passive is amorphous, the band gap (E_g) of oxide has to be replaced by the mobility gap (E'_g) accompanied with a tail of localized state into the band gap (E_g), and states within the gap contributed to process at lower energies.[4] Furthermore, the defective structure represents the mobile doping species and localized doping levels close to degeneracy in the band gap.[23] Therefore, the electronic structure within the energy range of the band gap can be influenced by localized donor bands or a high number of surface states (dangling band). All these additional states can affect the charge transfer and capacitance within the passive film.

Based on the above discussion, it is suggested that all passive films possessed the local variations in crystalline order or amorphous disorder to affect the semiconductor

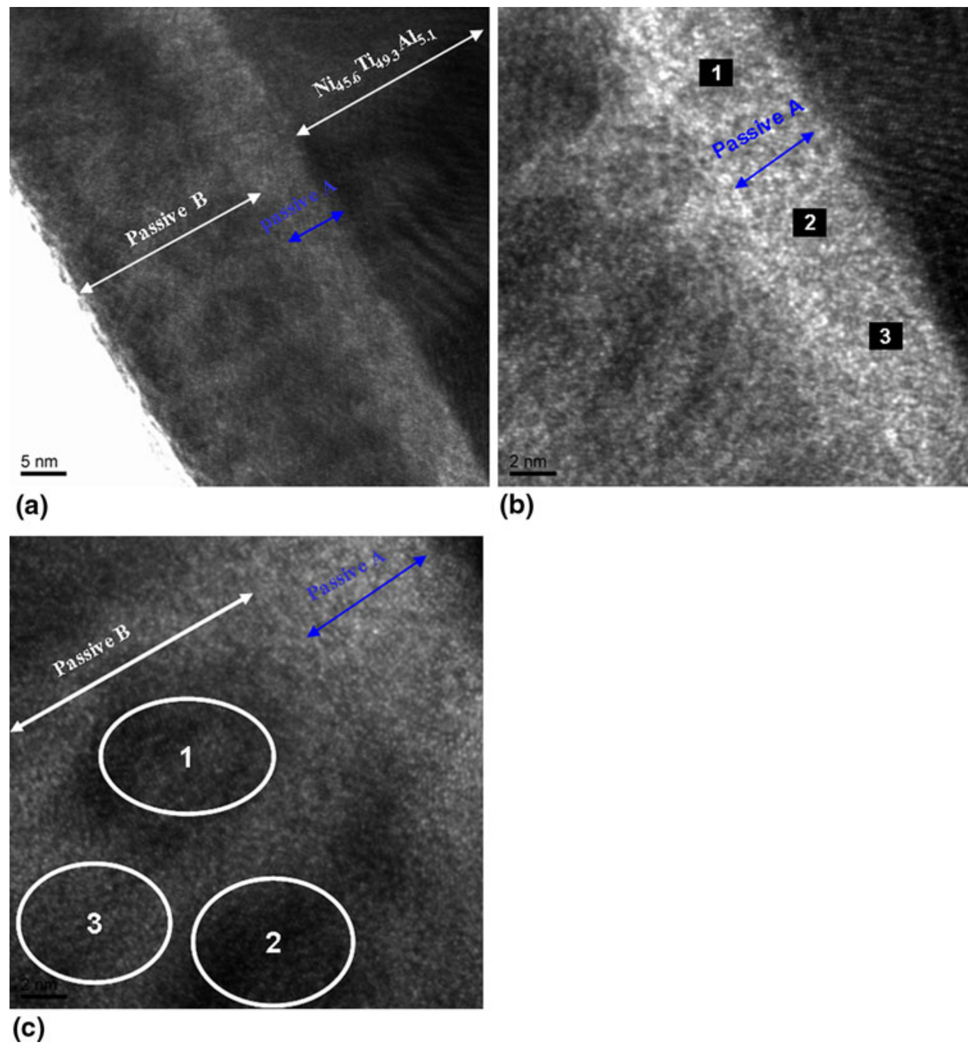

Fig. 3 HRTEM images of passive film on $Ni_{45.6}Ti_{49.3}Al_{5.1}$ after 1800 s of growth at 500 mV (vs. SCE). (a) Low magnification image in passive film; (b) high magnification image in passive A region; (c) high magnification image in passive B region

Table 1 EDS measurements of passive A layer (at.%)

	Ni	Ti	Al	O	Phase
1	5.5	41.2	6.4	46.7	Amorphous (Ti-rich oxide)
2	6.4	40.3	6.3	47	Amorphous (Ti-rich oxide)
3	6.7	41.3	7.2	44.8	Amorphous (Ti-rich oxide)

Table 2 EDS measurements of passive B layer (at.%)

	Ni	Ti	Al	O	Phase
1	*	16.3	22.3	61.4	Crystalline (Al-rich oxide)
2	*	18.3	22.4	59.3	Crystalline (Al-rich oxide)
3	*	37.2	6.3	56.5	Amorphous (Ti-rich oxide)

properties and electronic structure. Recently, Tromans[24] developed the thermodynamic evaluation for the effects of amorphism on passive films. According to melting point and enthalpy of fusion data for oxides, the maximum differences in the chemical free energy ($\Delta G_{a\text{-}c}$) between a crystalline and its fully amorphous oxides at 298 K can be estimated in transition metal systems. If the maximum differences in the chemical free energy ($\Delta G_{a\text{-}c}$) between a crystalline and its fully amorphous oxides at 298 K are large, it is possible for the passive layer to form a high degree of crystalline structure. The thermodynamic results can determine the stability of crystalline and amorphous phases in aqueous solutions. Therefore, Tromans[24] concluded that regions with the highest degree of amorphism produce the greatest instability and are likely to influence the sites which make the pitting corrosion and the localized breakdown of passive films. In this study, the microstructure showed that the crystalline and amorphous coexisted in the passive layer. The crystalline structure of Al-rich region was investigated in HRTEM. This phenomenon may be explained by the

above thermodynamic evaluation. For thermodynamic data of TiO_2, the melting point and enthalpy of fusion is 2130 K and 66.94 kJ/mol, respectively.[25] For Al_2O_3, the melting point and enthalpy of fusion is 2327 K and 111.1 kJ/mol, respectively.[25] The maximum differences in the chemical free energy ($\Delta G_{a\text{-}c}$) between a crystalline and its fully amorphous oxides at 298 K for TiO_2 and Al_2O_3 was calculated to be 57.57 and 96.87 kJ/mol, respectively.

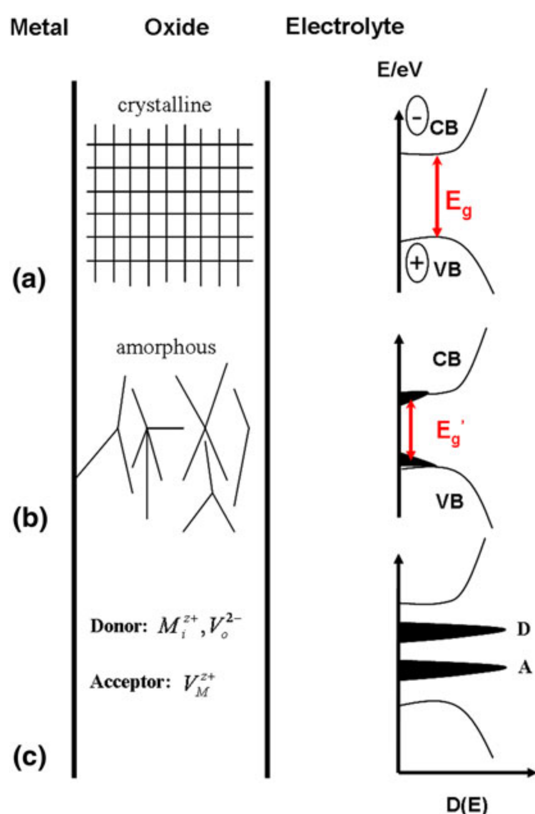

Fig. 4 Schematic plot of crystal structures and electronic states in the oxide film

4.2 Determination in Density of Defect and Diffusivity

The semiconductor properties of an oxide-electrolyte interface can be measured at high frequency immediately after the oxide was grown at specific film formation potential (U_{ff}). According to M-S theory,[26,27] the relationship between space charge capacitance (C_{sc}) and applied (E) can be described for n-type semiconductor.

$$\frac{1}{C_{sc}^2} = \frac{2}{\varepsilon\varepsilon_0 e N_d}\left(U - U_{fb} - \frac{k_b T}{e}\right), \quad \text{(Eq 6)}$$

where ε is the dielectric constant of the oxide; ε_0, the vacuum permittivity; q, the elementary charge (+e for electrons and −e for holes); N_d, the acceptor concentration; U, the applied potential; and U_{FB}, the flat potential. N_d can be determined from the slope of an experimental $1/C_{sc}^2$ versus U plot, while U_{fb} comes from Eq 6 by $1/C_{sc}^2 = 0$.

After stabilizing the passive film at a constant potential in a passive potential range (film formation potential) for 30 min, the capacitance-potential relationship was recorded at 1000 Hz. Figures 5(a) and 3(b) show the typical M-S plot (C^{-2} versus the applied potential U) obtained with formation of oxide films at 500 mV on $Ni_{50.5}Ti_{49.5}$ and $Ni_{45.6}Ti_{49.3}Al_{5.1}$ surface, respectively. There were two slopes existed in both samples. In order to obtain an accurate slope of an experimental $1/C_{sc}^2$ versus U plot, the fitting curve was selected from −0.6 to 0.2 V. The curves in Fig. 5(a) and (b) clearly represent n-type semiconductor behavior of the oxide film as its main defects creating the electron donor levels. The donor density of the oxide electrode on $Ni_{50.5}Ti_{49.5}$ and $Ni_{45.6}Ti_{49.3}Al_{5.1}$ surface were determined from M-S plots in the potential range between −0.6 to 0.2 V as 2.2×10^{21} cm^{-3}, and 1.4×10^{21} cm^{-3}, respectively. The flat-band potential of the oxide electrode $Ni_{50.5}Ti_{49.5}$ and $Ni_{45.6}Ti_{49.3}Al_{5.1}$ surface was also calculated by the intercept of $1/C_{sc}^2 = 0$ as −0.68 and −0.61 V, respectively.

The donor density (N_d) of the oxide film with various film formation potentials on the $Ni_{50.5}Ti_{49.5}$ and $Ni_{45.6}Ti_{49.3}Al_{5.1}$ surface was calculated from the slopes of M-S curves, as shown in Fig. 6(a) and (b), respectively. It was observed that N_d decreased exponentially with U_{ff}. The fitting curve in

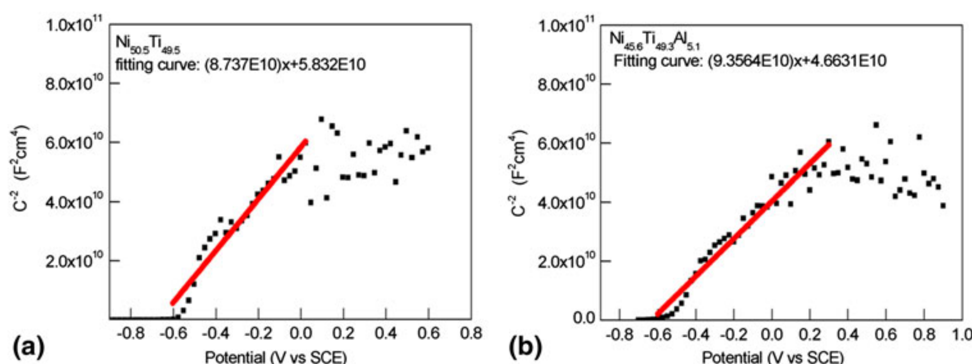

Fig. 5 Mott-Schottky plots as a function of testing potential for passive films on (a) $Ni_{50.5}Ti_{49.5}$ and (b) $Ni_{45.6}Ti_{49.3}Al_{5.1}$ formed after 1800 s of growth at 500 mV (vs. SCE) in chloride-containing solution

Fig. 6 was performed, and Eq 7 and 8 shows the optimum fit of the curve for $Ni_{50.5}Ti_{49.5}$ and $Ni_{45.6}Ti_{49.3}Al_{5.1}$, respectively.

$$N_d^{Ni_{50.5}Ti_{49.5}} = 9.62 \times 10^{20} + 9.01 \times 10^{21} \exp(-0.37U_{ff}) \quad \text{(Eq 7)}$$

$$N_d^{Ni_{45.6}Ti_{49.3}Al_{5.1}} = 3.62 \times 10^{20} + 2.11 \times 10^{21} \exp(-0.42U_{ff}) \quad \text{(Eq 8)}$$

The reciprocal passive film capacitance ($1/C_b$) is directly proportional to the oxide thickness. The thickness of passive film is taken as below:

$$L_{ss} = \frac{\varepsilon_0 \varepsilon}{C_b}, \quad \text{(Eq 9)}$$

where L_{ss} is the thickness of oxide; ε_0, the vacuum permittivity; ε, dielectric constant; and C_b, the capacitance of passive film. Equation 9 exhibits the relationship of capacitor. The capacitances of passive film on $Ni_{50.5}Ti_{49.5}$ and $Ni_{45.6}Ti_{49.3}Al_{5.1}$ versus film formation potential (U_{ff}) are indicated in Fig. 7(a) and (b), respectively. The values of film thickness (L_{ss}) as function of U_{ff} can be calculated by Eq 9. Obviously, there were two distinct regions in passive oxide corresponding to measurement of capacitance. The critical potential (U_{cr}) of the passive films on $Ni_{50.5}Ti_{49.5}$ and $Ni_{45.6}Ti_{49.3}Al_{5.1}$ were also determined as 0.57 and 0.76 V, respectively, as shown in Fig. 8. Under the critical film potential, the thickness of a film increased with increasing U_{ff}. However, the thickness of passive film grew only slightly when U_{ff} was above the critical potential. The maximum thickness of passivity at 3 V condition was 10.3 and 15.5 nm for $Ni_{50.5}Ti_{49.5}$ and $Ni_{45.6}Ti_{49.3}Al_{5.1}$, respectively.

A space charge layer was formed in the passive film, creating a strong electric field at the interface due to the doping level. The width of the space charge layer (d_{sc}) can be expressed as[28]:

$$d_{sc} = \left\{ \frac{2\varepsilon\varepsilon_0}{qN_d} \left(U_s - \frac{k_b T}{q} \right) \right\}^{1/2}, \quad \text{(Eq 10)}$$

where ε is the dielectric constant of the oxide; ε_0, the vacuum permittivity; q, the elementary charge; N_d, the doping concentration of the passive film; T, the temperature; k_b, the Boltzmann constant; and $U_s = (U_{app} - U_{FB})$, barrier height. The width of space charge layer versus U_s in various

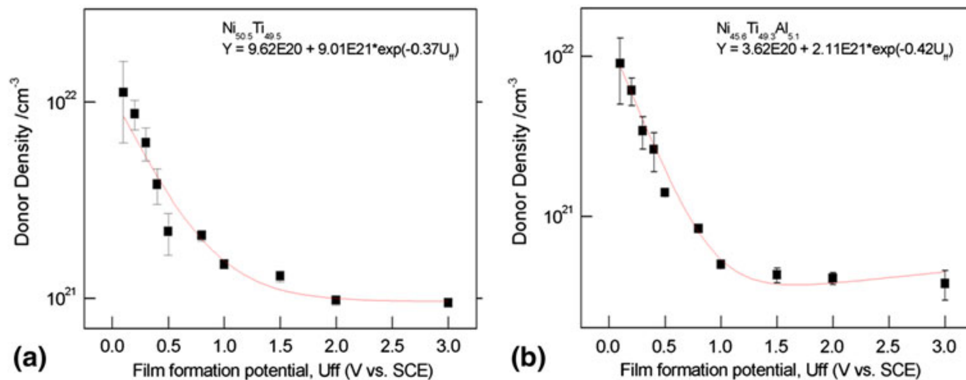

Fig. 6 Donor densities of the passive films formed on (a) $Ni_{50.5}Ti_{49.5}$ and (b) $Ni_{45.6}Ti_{49.3}Al_{5.1}$ in chloride-containing solution as a function of film formation potential. The *dots* are experimental measured data and the *solid line* is the fitting curve

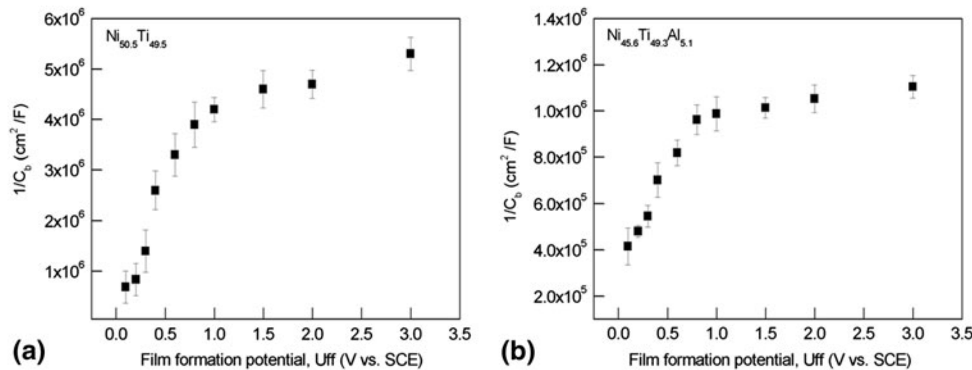

Fig. 7 Variation of the inverse of the barrier film capacitance ($1/C_b$) in the passive films of (a) $Ni_{50.5}Ti_{49.5}$ and (b) $Ni_{45.6}Ti_{49.3}Al_{5.1}$ as a function of film formation potential after 1800 s of growth

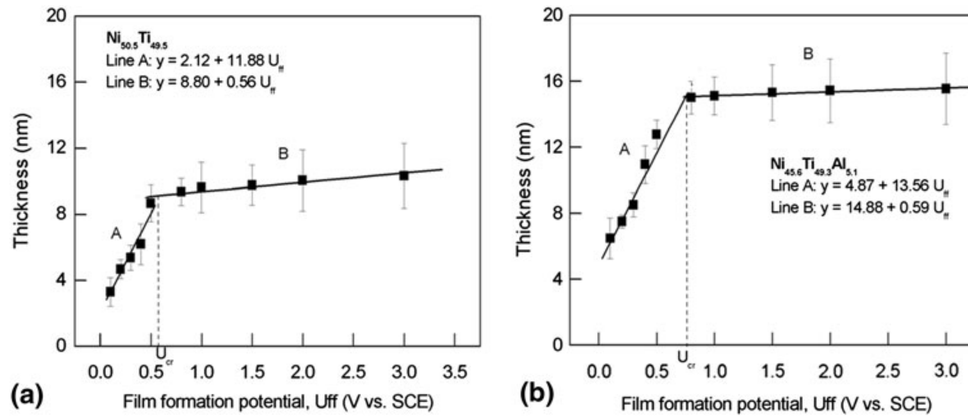

Fig. 8 Thickness of the passive films formed on (a) $Ni_{50.5}Ti_{49.5}$ and (b) $Ni_{45.6}Ti_{49.3}Al_{5.1}$ in chloride-containing solution as a function of film formation potential after 1800 s of growth. The *dots* are experimental measured data and the *solid line* is the fitting curve

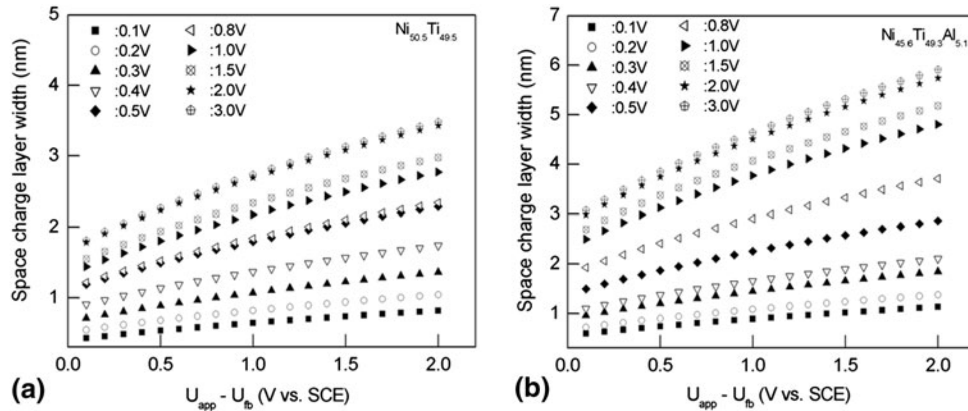

Fig. 9 Width of the space charge layer within the passive film of (a) $Ni_{50.5}Ti_{49.5}$ and (b) $Ni_{45.6}Ti_{49.3}Al_{5.1}$ in chloride-containing solution for different film formation potentials

film formation potentials (U_{ff}) was calculated from Eq 10, as shown in Fig. 9(a) and (b). With increasing U_s, the width of space charge layer was increased. The maximum width of space layer at 3 V film formation potential was estimated as 3.5 and 5.9 nm for $Ni_{50.5}Ti_{49.5}$ and $Ni_{45.6}Ti_{49.3}Al_{5.1}$, respectively.

The flux of oxygen vacancies, J_v, through the passive film may be expressed by Nernst-Planck equation:

$$J_v = -D_v\left(\frac{\partial C_v}{\partial x}\right) + 2KD_vC_v, \quad \text{(Eq 11)}$$

where J_v is the flux of vacancies; D_v, the diffusivity of oxygen vacancies for n-type semiconductor; $K = V_0F/RT$; and V_0 is the mean electric field strength. The donor density calculated from M-S fitting curves was vacancy concentration at the metal/film interface.

$$C_v(L_{ss}) = N_d = \omega_1 \exp[-bU_{ff}] + \omega_2, \quad \text{(Eq 12)}$$

where C_v (L_{ss}) is the concentration of vacancies at the metal/film interface; N_d, the donor density; U_{ff}, the film formation potential. The parameters ω_1 and b are determined by Eq 7 and 8 for passive films $Ni_{50.5}Ti_{49.5}$ and $Ni_{45.6}Ti_{49.3}Al_{5.1}$, respectively.

ω_2 is given by[5]

$$\omega_2 = \frac{J_vRT}{zFV_0D_v}, \quad \text{(Eq 13)}$$

where $J_v = -i_{ss}/2e$; i_{ss}, is the steady-state current density; R, the gas constant; T, the temperature; and F, the Faraday constant.

To obtain a steady-state current density (i_{ss}) through passive film on $Ni_{50.5}Ti_{49.5}$ and $Ni_{45.6}Ti_{49.3}Al_{5.1}$, potentiostatic polarization tests were carried out. The value of i_{ss} measured after passivation for 30 min were achieved as a function of film formation potential in Fig. 10. The value of i_{ss} for $Ni_{50.5}Ti_{49.5}$ and $Ni_{45.6}Ti_{49.3}Al_{5.1}$ were estimated to be 5.62×10^{-6} and 2.45×10^{-6} A/cm^2, respectively. It is evident that the value of i_{ss} is not dependent on film formation potential. The polarization curve of the passive film revealed that the measured passive current was independent of the electrode potential. In addition, the

value of electric field strength (V_0) can be calculated from Eq 14[5] using the slope of L_{ss} versus U_{ff} in Fig. 8.

$$L_{ss} = \frac{1}{V_0}(1-\alpha)U_{ff} + B, \qquad \text{(Eq 14)}$$

where α represents the polarizability of the barrier layer solution interface, and B is a constant related to the thickness of the film at a formation potential of 0 V. For iron, the value of α was calculated to be 0.45.[29] For WO_3, the average value for α was about 0.3.[13] In this study, the value of α was assumed to be 0.4.

Table 3 shows the parameters calculated to obtain D_v by Eq 13. In the calculation of thickness, there were two regions of growth for passive films, as shown in Fig. 8. Therefore, the diffusivity (D_v) (line A region) on $Ni_{50.5}Ti_{49.5}$ and $Ni_{45.6}Ti_{49.3}Al_{5.1}$ was calculated to be 5.50×10^{-16} and 3.87×10^{-16} cm^2/s, respectively, under the critical potential (U_{cr}). Besides, the diffusivity (D_v) of passive film (line B region) on $Ni_{50.5}Ti_{49.5}$ and $Ni_{45.6}Ti_{49.3}Al_{5.1}$ was also determined above the critical potential (U_{cr}) to be 3.11×10^{-17} and 2.93×10^{-17} cm^2/s, respectively. In literature, the discussion of the diffusivity of point defects in the passive film on carbon steels,[15,30] Fe[16] and W[13,31] was addressed by electrochemical methods. In fact, it is difficult to directly compare the values of diffusivity in those studies because of the different electrolytes used, i.e., pH 9.3 borate buffer,[15] pH 8.5 buffer,[16] HNO_3 solution,[30] and various materials used. In Luo and coworkers[15] and Guo et al.'s study,[30] the value of diffusivity was determined as 10^{-16} to 10^{-15} and 9.8×10^{-17} cm^2/s, respectively, on carbon steel. In iron material, the diffusivity was calculated to be 1.69×10^{-20} cm^2/s by Ahn and Kwon.[16] In this study, the value of diffusivity was 10^{-16} to 10^{-17} cm^2/s for $Ni_{50.5}Ti_{49.5}$ and $Ni_{45.6}Ti_{49.3}Al_{5.1}$. In the literature,[15,16,30] there are orders of magnitude difference in diffusivity among reported data. The reason for this discrepancy may be as follows. First, differences among calculated diffusivities of defects may be caused from the use of equations. Cheng and coworkers[15] used the low field approximation to obtain the diffusivity of point defect on carbon steel with 10^{-16} to 10^{-15} cm^2/s. In this study, the low field approximation was adopted to calculate D_v, since HRTEM images showed that the passive layer consisted of amorphous and crystalline structure. The half-jump distance in the high-field approximation is not a constant to calculate D_v, and the passive structure would affect the diffusivity of an oxygen vacancy due to half-jump distance. This consideration is important because the transport number and conduction mechanism in the growth of oxide films could vary between amorphous and crystalline phases.[13] It is probably the different film formation times are a second reason. The formation time was 2 and 4 h in Cheng and coworkers[15] and Guo et al.,[30] respectively. In Ahn and Kwon's study,[16] the film formation time was 24 h to reach a steady-state condition. The film formation time was short because the current flow through passive film at this stage was much higher than at the steady state. Therefore, the diffusivity could be overestimated. For film formation time of $Ni_{50.5}Ti_{49.5}$ and $Ni_{45.6}Ti_{49.3}Al_{5.1}$, 30 min was selected to form the passive film to determine the value of diffusivity with 10^{-16} to 10^{-17} cm^2/s. In fact, the film formation time may be too short to achieve a steady state in chloride solution.

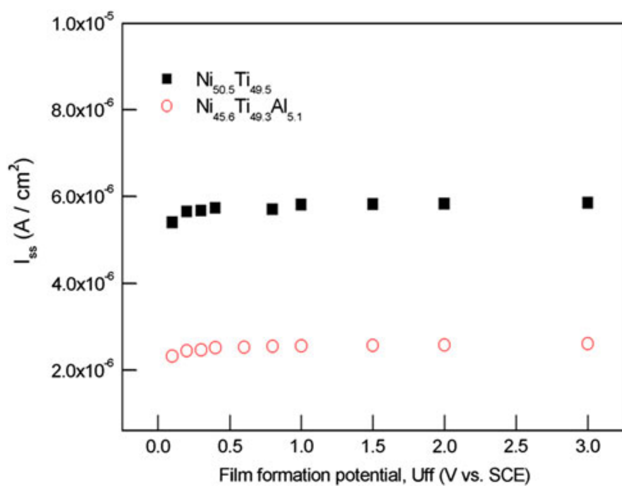

Fig. 10 Steady-state current density through passive films vs. various film formation potentials formed on $Ni_{50.5}Ti_{49.5}$ and $Ni_{45.6}Ti_{49.3}Al_{5.1}$ for 1800 s

Table 3 Calculated parameters to obtain D_v of the passive films on $Ni_{50.5}Ti_{49.5}$ and $Ni_{45.6}Ti_{49.3}Al_{5.1}$

	$Ni_{50.5}Ti_{49.5}$	$Ni_{45.6}Ti_{49.3}Al_{5.1}$
I_{ss}, A/cm^2	5.62×10^{-6}	2.45×10^{-6}
α	0.4	0.4
V_0, V/cm (line A)	5.05×10^{5}	6.92×10^{5}
V_0, V/cm (line B)	8.93×10^{6}	9.16×10^{6}
w_2	9.62×10^{20}	3.62×10^{20}
D_v, cm^2/s (line A)	5.50×10^{-16}	3.87×10^{-16}
D_v, cm^2/s (line B)	3.11×10^{-17}	2.93×10^{-17}

5. Conclusion

By employment of the PDM, it was concluded that the interfacial equilibrium due to the transport vacancies in the passive film for NiTi and NiTiAl was governed by anion transmission, which was attributed to the transport of the $V_{\ddot{O}}$ (oxygen vacancies) through the film. The diffusivity of oxygen vacancy was evaluated in the range of 10^{-16} to 10^{-17} cm^2/s. According to microstructural observation, the degree of crystalline structure may affect the electronic level and the diffusivity within the passivation layer. The chemical free energy ($\Delta G_{a\text{-}c}$) between a crystalline and its fully amorphous oxides should be considered to develop the anti-corrosion material. The higher degree of crystalline structure can have a lower diffusivity of oxygen vacancy to suppress the migration of oxygen vacancy. On the basis of

thermodynamic evaluation and microstructure evidence, Al_2O_3 has a higher degree of crystalline structure than that of TiO_2. Therefore, the addition of aluminum into NiTi can induce crystalline structure to suppress the transport of $V_{\ddot{O}}$, leading to better anti-corrosive properties.

Acknowledgment

The support of work from the National Science Council, Taiwan, under Contract No. NSC 96-2221-E-007-093-MY3 is appreciated.

References

1. S. Ningshen, U.K. Mudail, V.K. Mittal, and H.S. Khatak, Semiconducting and Passive Film Properties of Nitrogen-Containing Type 316LN Stainless Steels, *Corros. Sci.*, 2007, **49**, p 481-496
2. C.O.A. Olsson and D. Landolt, Passive Films on Stainless Steels—Chemistry, Structure and Growth, *Electrochim. Acta*, 2003, **48**, p 1093-1104
3. V. Battaglia and J. Newman, Modeling of a Growing Oxide Film: The Iron/Iron Oxide System, *J. Electro. Soc.*, 1995, **142**, p 1423-1430
4. F.P. Fehlner and N.F. Mott, Low-Temperature Oxidation, *Oxidat. Met.*, 1970, **2**, p 59-99
5. E. Sikora, J. Sikora, and D.D. Macdonald, A New Method for Estimating the Diffusivities of Vacancies in Passive Films, *Electrochim. Acta*, 1996, **41**, p 783-789
6. J. Frenkel, A Perfect Lattice Approach to Nonstoichiometry, *Z. Phys.*, 1926, **35**, p 652-658
7. C.Y. Chao, L.F. Lin, and D.D. Macdonald, A Point Defect Model for Anodic Passive Films, *J. Electro. Soc.*, 1981, **128**, p 1187-1194
8. C.Y. Chao, L.F. Lin, and D.D. Macdonald, A Point Defect Model for Anodic Passive Films, *J. Electro. Soc.*, 1981, **128**, p 1194-1198
9. D.D. Macdonald, The Point Defect Model for the Passive State, *J. Electro. Soc.*, 1992, **139**, p 3434-3449
10. D.D. Macdonald, Passivity—The Key to Our Metals-Based Civilization, *Pure Appl. Chem.*, 1999, **71**, p 951–978
11. N. Sato, The Potentials of Mixed Electrodes of Corrodible Metal and Metal Oxide, *Corros. Sci.*, 2000, **42**, p 1957-1973
12. M. Pontinha, S. Faty, M.G. Walls, M.G.S. Ferreira, and M.D.C. Belo, Electronic Structure of Anodic Oxide Films Formed on Cobalt by Cyclic Voltammetry, *Corros. Sci*, 2006, **48**, p 2971-2986
13. G. Vazquez and I. Gonzalez, Diffusivity of Anion Vacancies in WO_3 Passive Films, *Electrochim. Acta*, 2007, **52**, p 6771-6777
14. M. Bojinov, The Ability of a Surface Charge Approach to Describe Barrier Film Growth on Tungsten in Acidic Solutions, *Electrochim. Acta*, 1997, **42**, p 3489-3498
15. Y.F. Cheng, C. Yang, and J.L. Luo, Determination of the Diffusivity of Point Defects in Passive Films on Carbon Steel, *Thin Solid Films*, 2002, **416**, p 169-173
16. S.J. Ahn and H.S. Kwon, Diffusivity of Point Defects in the Passive Film on Fe, *J. Electroanalytic Chem.*, 2005, **579**, p 311-319
17. K.T. Liu and J.G. Duh, Grain Size Effects on the Corrosion Behavior of $Ni_{50.5}Ti_{49.5}$ and $Ni_{45.6}Ti4_{9.3}Al_{5.1}$ Films, *J. Electroanalytic Chem.*, 2008, **618**, p 45-52
18. A.J. Bard and L.R. Fauljner, *Electrochemical Methods Fundamentals and Applications*, 2nd ed., John Wiley & Sons, USA, 2001
19. L. Zhang and D.D. Macdonald, On the Transport of Point Defects in Passive Film, *Electrochim. Acta*, 1998, **43**, p 679-691
20. J. Troe and R.T. Watson, Evaluated Kinetic Data on Gas Phase Addition, *J. Phys. Chem. Ref. Data*, 1982, **11**, p 323-343
21. K. Ghosh and H.P. Maruska, Photoelectrolysis of Water in Sunlight with Sensitized Semiconductor Electrodes, *J. Electrocchem. Soc.*, 1977, **124**, p 1516-1522
22. M.W. Peterson and B.A. Parkinson, Photoelectrochemical Investigation of Several II-IV-V2 Semiconducting Glasses, *J. Electrochem. Soc.*, 1986, **133**, p 2538-2541
23. M.H. Dean and U. Stimming, Capacity of Semiconductor Electrodes with Multiple Bulk Electronic States. Part I. Model and Calculations for Discrete States, *J. Electroanalytic Chem.*, 1986, **228**, p 135-151
24. D. Tromans, Thermodynamic Evaluation of the Effects of Amorphism on Film Breakdown and Pitting Initiation, *J. Electrocchem. Soc.*, 2005, **152**, p B460-B469
25. I. Bharin and G. Platzki, *Thermochemical Data of Pure Substances*, Vol I, and II, 3rd ed., VCH Publishers Inc, New York, 1995, p 48-1692
26. W. Schottky, Semiconductor Theory of the Blocking Layer, *Z. Phys. Chem.*, 1939, **113**, p 367-371
27. N.F. Mott, Theory of the Oxidation of Metals, *Proc. Roy. Soc. Londer Ser., A*, 1939, **171**, p 27
28. H. Tsuchiya, J.M. Macak, A. Ghicov, A.S. Rader, L. Taveira, and P. Schmuki, Characterization of Electronic Properties of TiO_2 Nanotube Films, *Corros. Sci.*, 2007, **49**, p 203-210
29. D.D. Macdonald and M.U. Macdonald, Theory of Steady-State Passive Films, *J. Electrochem. Soc.*, 1990, **137**, p 2395-2402
30. X.P. Guo, Y. Tomoe, H. Imaizumi, and K. Katoh, The Electrochemical Behavior and Impedance Characteristics of the Passive Film on Carbon Steel in Nitric Acid Solutions, *J. Electroanalytic Chem.*, 1998, **445**, p 95-103
31. Y.M. Zeng and J.L. Lou, Electronic Band Structure of Passive Film on X70 Pipeline Steel, *Electrochim. Acta*, 2003, **48**, p 3551-3562